Mergers in Supercell Environments. Part I: Conceptual models of mechanisms governing merger outcomes

R. M. Hastings, * Y. P. Richardson, P. M. Markowski
Department of Meteorology, The Pennsylvania State University, University Park, Pennsylvania

J. M. Wurman
Center for Severe Weather Research, Boulder, Colorado

C. C. Weiss
Atmospheric Sciences Group, Department of Geosciences, Texas Tech University, Lubbock, Texas

1. Introduction

Storm mergers involving supercells present a current challenge in severe storms forecasting, as the long-term (∼40 minutes) effect of a merger on storm morphology is not known. Some mergers result in stronger storms, while others lead to the annihilation of both storms. In particular, we are interested in the resulting storm type, subsequent persistence, and rotational characteristics.

In Part I of this study, we use idealized numerical models to identify four general types of mergers. Comparison of the results from these experiments to real-world observations from VORTEX2 and of the 19–20 April 1996 outbreak seems to validate three of these types. The remaining type resembles similar real-world mergers in some aspects, but some significant distinctions necessitate further modeling work. In Part II, we examine some mechanisms that may contribute to near-surface vortex intensification during the merger process.

In order for this research to be useful for the operational community, a definition of merger based on reflectivity has been adopted. Two cells (i.e., reflectivity maxima) merge when they join at a high reflectivity contour relative to their respective pre-merger maxima, with the separate maxima no longer remaining. To limit the scope of this study, we are exclusively interested in mergers between supercells or between supercells and ordinary cells.

2. Methods

Our investigation of this problem takes two approaches: numerical and observational. In this section, we introduce the numerical methods. The observations will be discussed in Section 5.

a. Idealized numerical models

Simulations were carried out using the non-hydrostatic, fully-compressible cloud model CM1r15 (Bryan and Fritsch 2002), on a 120×120×18.375 km grid, with a uniform horizontal grid spacing of 500 m and a vertical grid that stretches from 50 m to 700 m. The thermodynamic base state represents a warm-season day during which deep convection might be supported (Weisman and Klemp 1982), with surface-based convective available potential energy of about 1900 J kg^{-1} and convective inhibition slightly below 50 J kg^{-1} (Fig. 1). The base state wind profile is a semicircle with 17.5 m s^{-1} easterlies at the surface, veering to equal magnitude westerlies at 5 km, and constant winds above 5 km (Fig. 2, Weisman and Klemp 1984). Lateral boundary conditions are open-radiative. A Rayleigh "sponge" layer starts at 14 km. Microphysics is parameterized with the double-moment Morrison scheme, and subgrid-scale turbulence is parameterized with the 1.5-order TKE closure. Surface physics, terrain, and radiation are not included.

Convection is initiated using 2-K warm bubbles. The first bubble is included with the initial conditions. A second bubble is introduced 3300 s into the simulation at a location where the resulting storm will collide with the original storm. The location is varied in order to vary the configuration of the merger as well as the relative maturity of the storms. In all cases, the new storm is pre-supercellular when the merger begins.

3. Results of numerical experiments

A total of 36 runs varying the placement of the second bubble yields a suite of simulations that can be divided into four general types. These types should be understood to represent a spectrum of possibilities rather than completely separate categories.

Type I: Forward-flank collision, resulting in a bow echo

The first type of merger occurs when the new cell moves into the forward-flank precipitation of the older cell. The new cell is beginning to develop precipitation as it encoun-

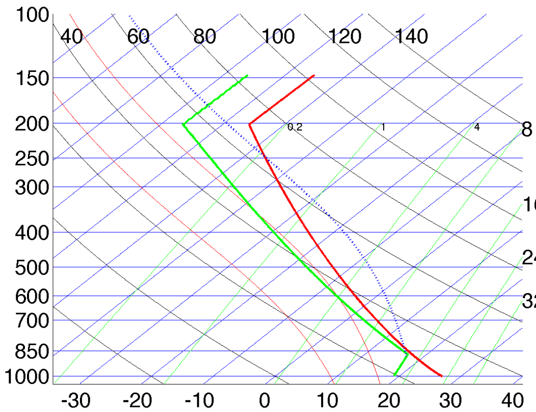

FIG. 1. Skew-T log-p diagram for base state.

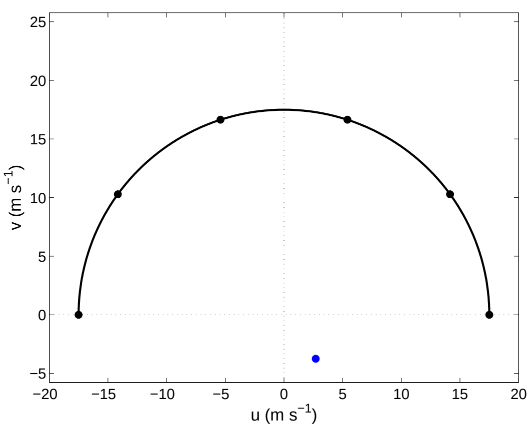

FIG. 2. Skew-T and log-p hodograph for base state. Black dots every 1 km on hodograph, blue circle on hodograph markes motion of isolated (control) storm.

ters the mature supercell (Fig. 3, top). The resulting increase in hydrometeors is followed, minutes later, by a cold pool surge between the original updrafts. Upscale growth accompanying this surge leads to a region of contiguous updraft (Fig. 3, middle), with the system subsequently reorganizing as a bow echo (Fig. 3, bottom).

Type II: Forward-flank collision, resulting in a classic supercell

If the second cell is mature enough to produce a more substantial cold pool as it moves into the forward flank, the event proceeds differently from the previous type (Fig. 4). The outflow from the new cell cuts off the warm, moist inflow to the original cell, causing the older cell to dissipate. The new storm continues, maturing into a supercell in the

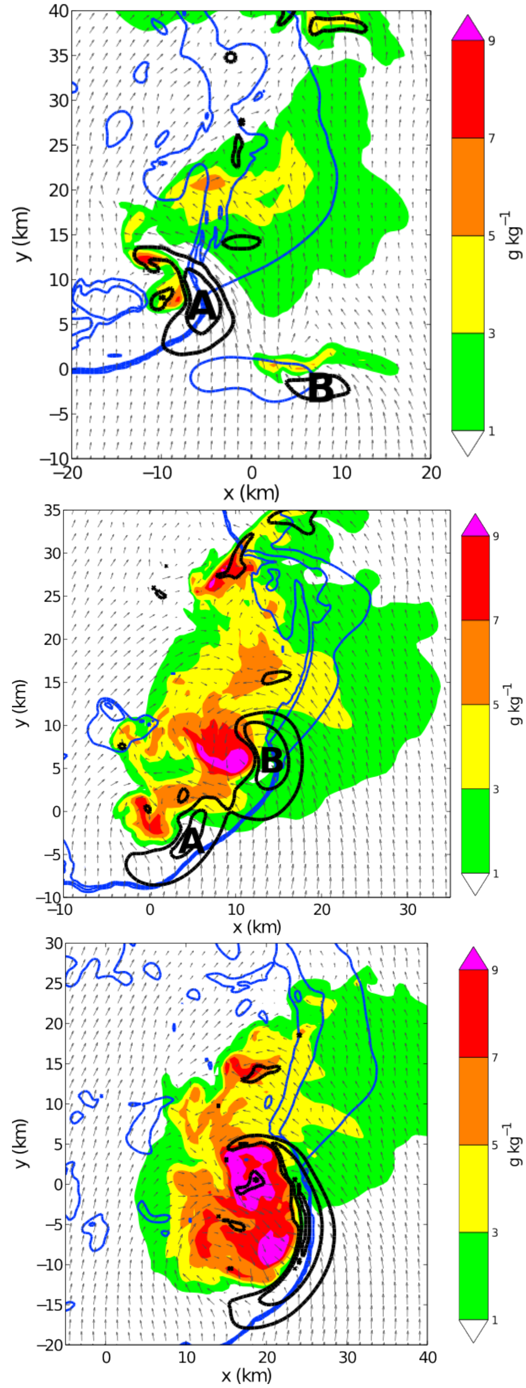

FIG. 3. Type I merger at 90, 135, and 170 min at the top, middle, and bottom, respectively. Precipitation mixing ratio at z = 2.5 km color-shaded, updraft at z = 2.5 km contoured in black every 10 m s^{-1} starting at 5 m s^{-1}, Density potential temperature perturbation at z = 25 m contoured in blue every -2 K starting at -1 K. Original (new) cell marked as A (B).

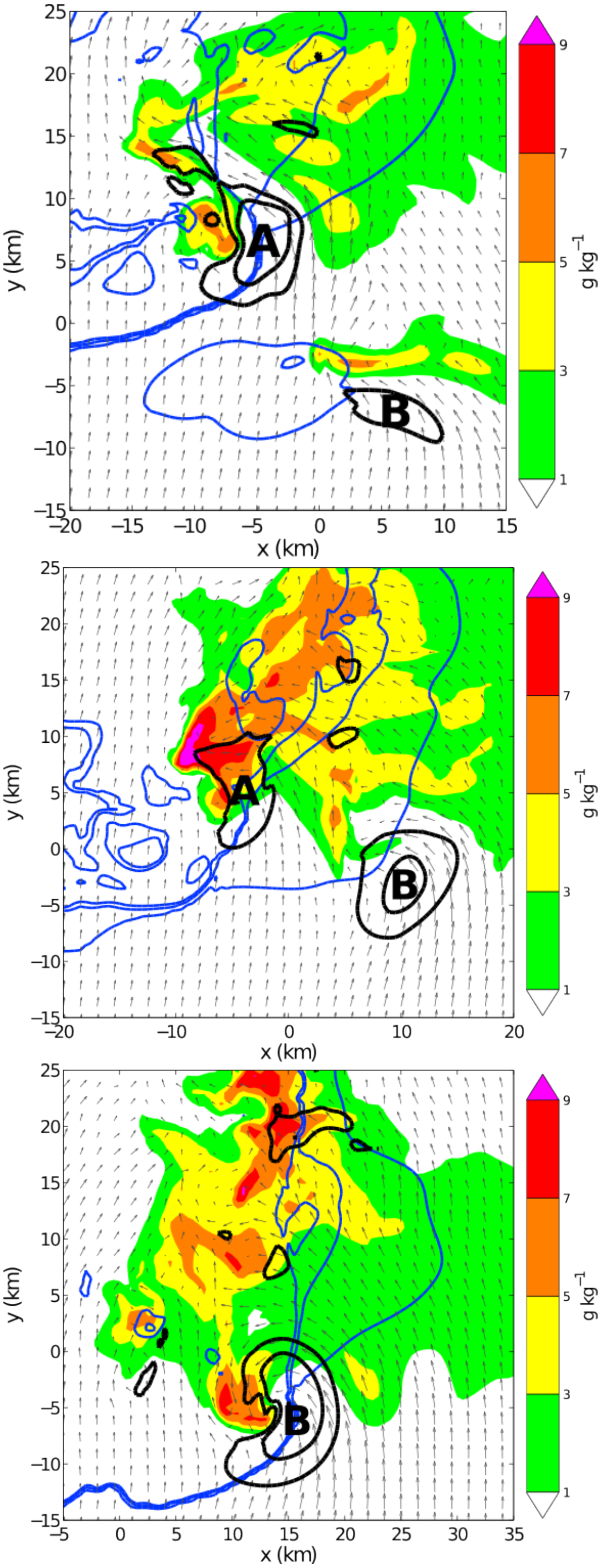

Fig. 4. As Fig. 3, for Type II at 94 (top), 110 (middle), and 115 (bottom) min.

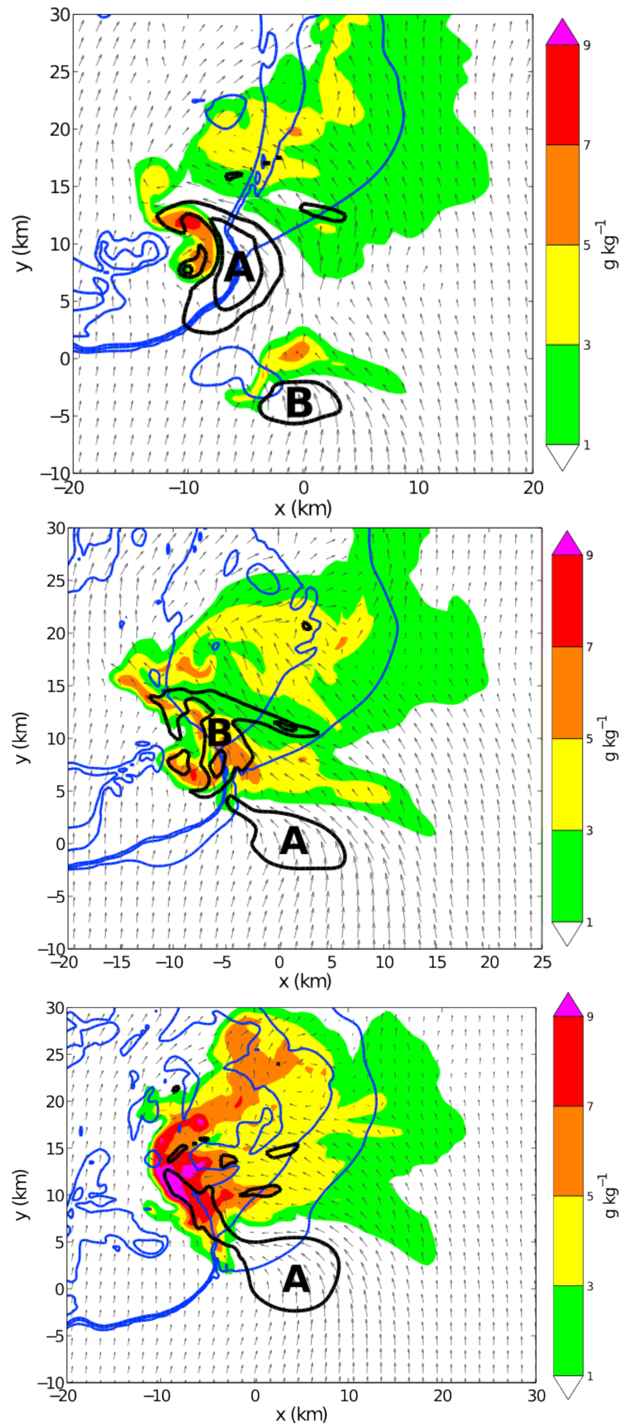

Fig. 5. As Fig. 3, for Type III at 87 (top), 96 (middle), and 104 (bottom) min.

same way an isolated cell does.

Type III: Updraft collision, resulting in a supercell

The third type of merger occurs with a collision between cell updrafts (Fig. 5). It is characterized by direct interactions between the updrafts, with cold pool-updraft interactions playing a secondary role. These updraft-updraft interactions may take the form of a fusion beween the updrafts, joining at a relatively high contour (i.e., 15–30 m s^{-1}), or a replacement, with a "bridge" joining them at a relatively low contour (5–15 m s^{-1}), followed by the dissipation of the original updraft and strengthening of the new one. In either case, the system continues with a structure closer to the classic supercell type on the high-precipitation (HP) to classic spectrum. In some cases, especially those that share characteristics with the Type II mergers, the Type III mergers resemble cycling mesocyclogenesis.

Type IV: Rear-flank collision, resulting in an HP supercell

Figure 6 shows an example of a Type IV merger. The new updraft encounters the rear-flank downdraft (RFD) of the original cell. The cold pool surges outward between the updraft, with subsequent upscale growth joining the separate updrafts. This process resembles that of Type I, except instead of re-organizing into a bow echo, the system becomes an HP supercell, with cycling mesocyclogenesis. The storms resulting from Type IV mergers have significantly stronger low-level mesocyclones than the control storm and any of the other mergers.

4. Role of the cold pool in Type I and Type IV mergers

The morphology of Type I and Type IV mergers are strikingly similar. In both cases, an outflow surge pushes out between the updrafts, forcing the growth of new updraft connecting the originally separate cells. However, Type I mergers result in bow echoes, while Type IV mergers result in HP supercells. The key difference between the mergers that governs this outcome is the strength of the cold pool.

Rotunno et al. (1988) defined cold pool strength as

$$c^2 = -2\int_{z=0}^{z=H} B\,dz, \qquad (1)$$

where H is the depth of the cold pool, in this case taken to be the height at which the buoyancy is -0.1 m s^{-2} (roughly corresponding to the -3 K density potential temperature perturbation). We expect this to be related to the vertically integrated hydrometeor content,

$$VIH = \int_{z=0}^{z=4\text{ km}} q_r + q_g + q_s\,dz, \qquad (2)$$

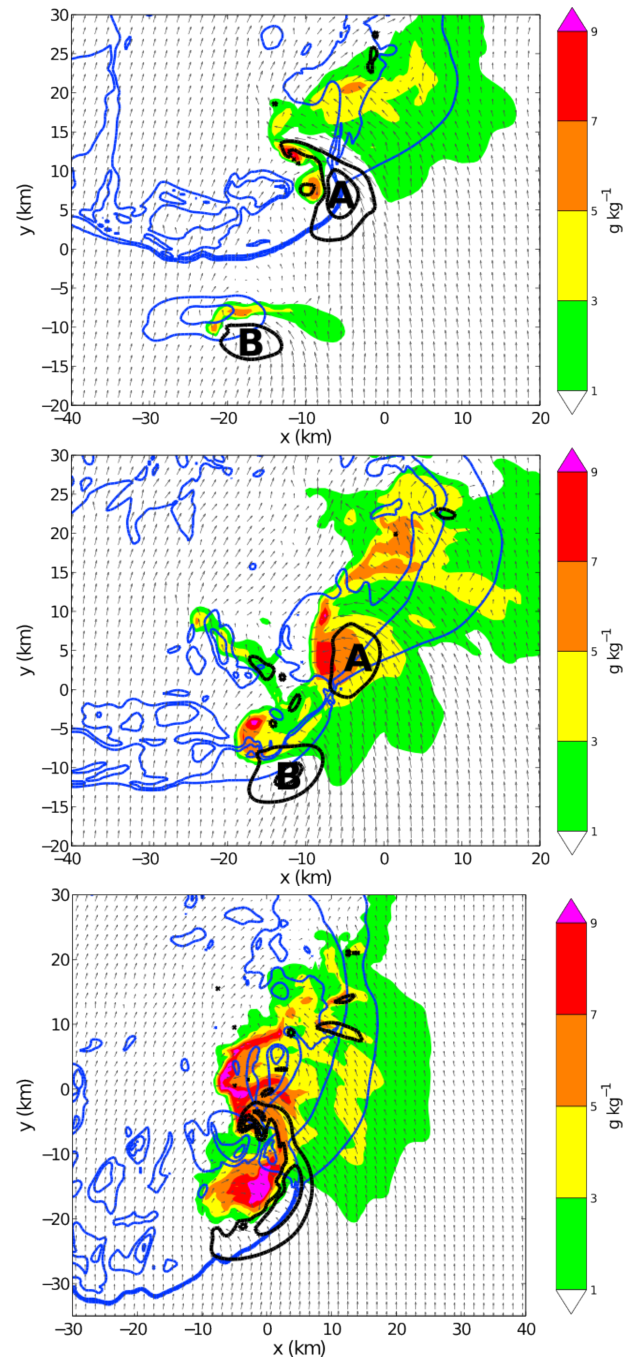

Fig. 6. As Fig. 3, for Type IV at 90 (top), 110 (middle), and 160 (bottom) min.

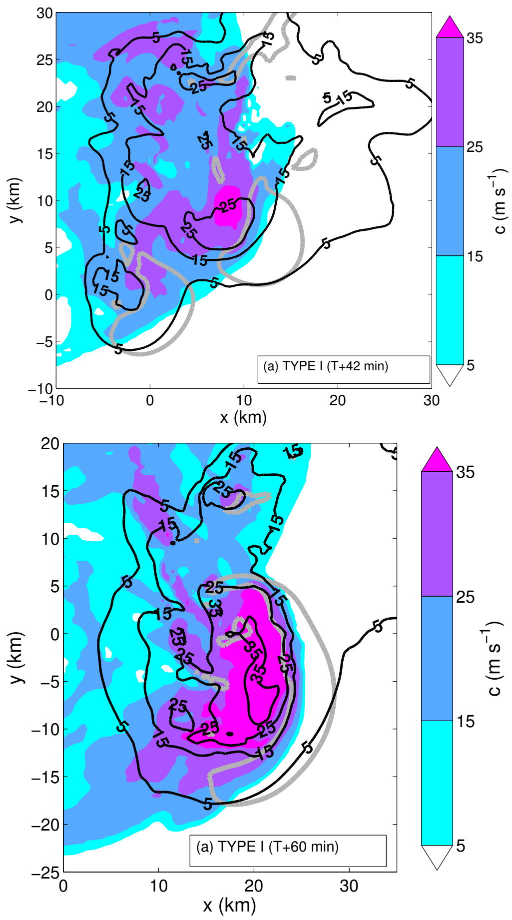

Fig. 7. Cold pool strength (color shaded) and vertically integrated hydrometeor content (black contours, every 10 mm beginning at 5 mm), for a Type I merger (a) just before the updrafts join and (b) after the storm has reorganized. 10 m s^{-1} updraft at $z = 2.5$ km contoured in gray.

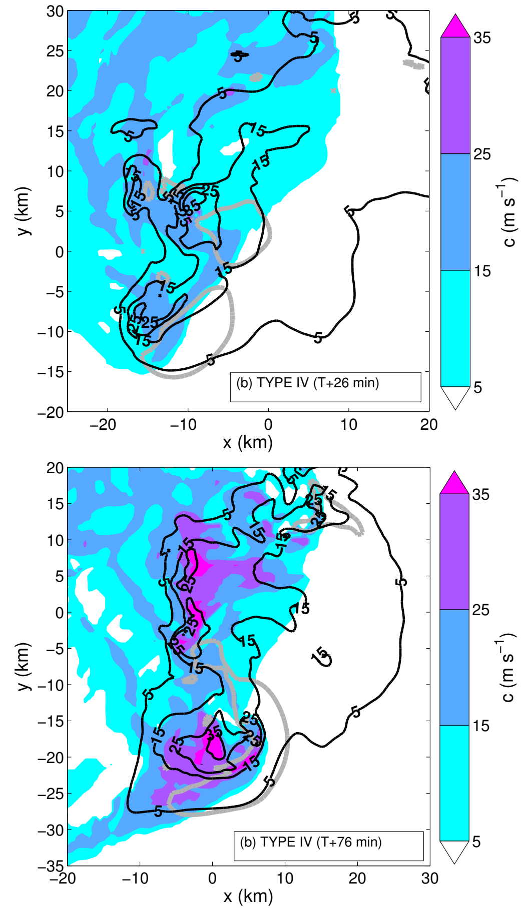

Fig. 8. As Fig. 7, for Type IV mergers.

where ρ_d is the density of dry air, ρ_w is the density of liquid water, and q_r, q_g, and q_s are the rain, hail, and snow mixing ratios, respectively.

Figures 7 and 8 compare the cold pool strength and VIH for mergers Type I and Type IV, respectively. The difference between the two is immediately evident: The cold pool for Type I mergers is significantly stronger than for Type IV mergers. The correspondence between higher VIH values and greater cold pool strengths is also evident. The stronger cold pool of Type I results from the greater concentration of precipitation directly behind the updraft. For Type IV mergers, the precipitation is distributed broadly, resulting in a weaker cold pool.

To understand the distribution of precipitation during the merger, we first note that, in an isolated storm, the precipitation primarily falls to the north and northeast of the updraft. This is forward relative to the motion of pre-supercellular storms, and left relative to the motion of supercells. A Type I merger occurs when the new storm moves into the left flank of the original storm, thus depositing its precipitation in the already precipitation-rich area of the original storm. Type IV mergers, on the other hand, occur when precipitation from the new storm falls into the the re RFD of the original, where the total volume of precipitation is much less than that in the left flank. The stronger cold pools are due to the greater number of hydrometeors, which decreases buoyancy through a combination of precipitation loading and evaporative cooling. This mechanism is identical to that identified by Finley et al. (2001) as playing the dominant role in a simulation of the an HP supercell undergoing multiple mergers before transitioning to a bow echo.

5. Comparison to real-world observations

The validity of the conceptual models presented in the previous section may be tested by comparison with observed cases of mergers. These cases are drawn from a tornado outbreak in central Illinois on 19–20 April 1996 and from the Second Verification of the Origins of Rotation in

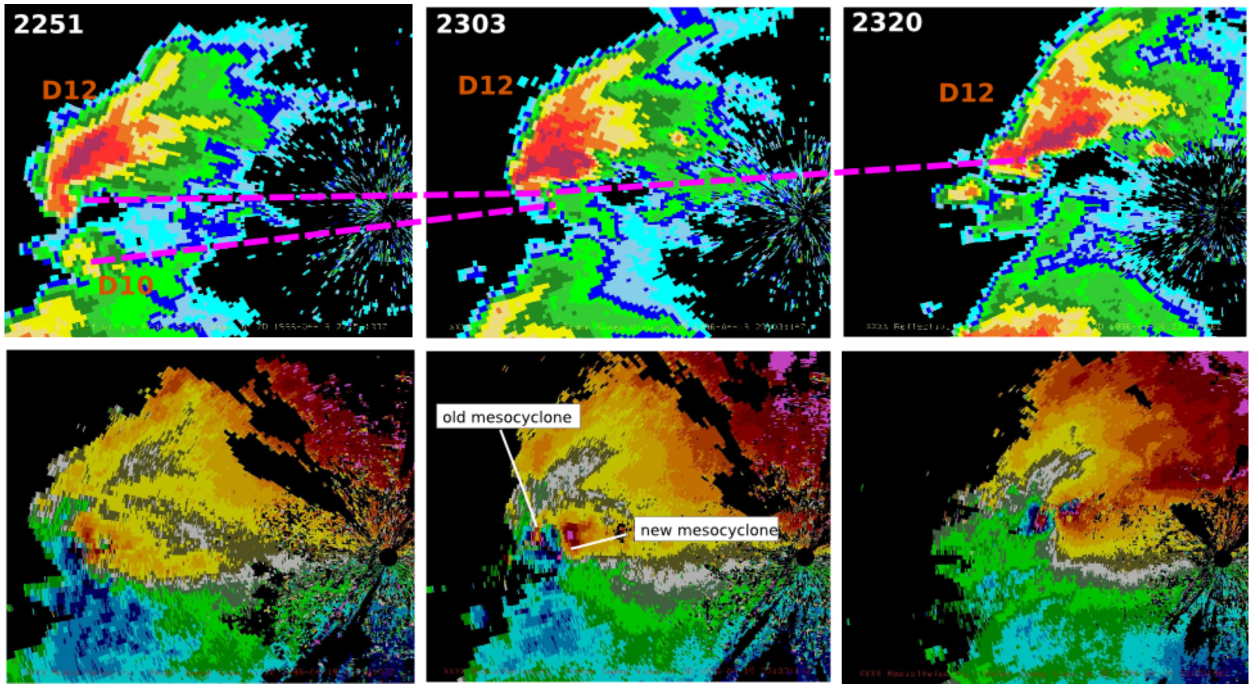

Fig. 9. Reflectivity (top) and velocity (bottom) from KILX showing Type III merger on 19 April 1996 at 2303. Note the resemblance to cyclic mesocyclogenesis, possibly due to the development of a mesocyclone in D10 as it merges into D12. Two brief tornadoes occurred during this merger, at 2307 (causing F2 damage) and 2317 (causing F1 damage).

Tornadoes Experiment (VORTEX2).

In order to qualify for comparison to the numerical results, at least one of the merging cells must have a mesocyclone, and the merger must take place away from any obvious air mass boundaries, such as can be identified with radar fine-lines or surface observations.

For the Illinois outbreak, radar data from KDVN, KILX, and KSLX are used. During VORTEX2, a wider variety of instrumentation is available for high-resolution observations. Six platforms in particular are most heavily used for this study: The X-band Dopplers On Wheels (DOW6 and DOW7, Wurman et al. 1997), the C-band Shared Mobile Atmospheric Research and Teaching Radars (SR1 and SR2, Biggerstaff et al. 2005), National Severe Storms Laboratory mobile mesonets (Straka et al. 1996), and Texas Tech University StickNets (Weiss and Schroeder 2008). The latter two platforms provide surface observations of temperature, relative humidity, wind speed and direction, and pressure. The VORTEX2 radar data are edited to remove ground clutter, dealiased, and objectively analyzed to a regular grid using a two-pass Barnes filter (Majcen et al. 2008). For all objective radar analyses, the convergence parameter (γ) is 0.3. Both the smoothing parameter (κ) and the grid spacing are determined using the recommendations of Pauly and Wu (1990), with the grid spacing between $\Delta/3$ and $\Delta/2$, where Δ is the coarsest data spacing in the region of interest, and $\kappa = (1.33\Delta)^2$. A storm motion correction is used for each volume, with the storm motion determined by the motion of a feature of interest (e.g., the mesocyclone).

19–20 April 1996 outbreak in central Illinois

Lee et al. (2006a,b) have previously examined the Illinois tornado outbreak in great detail. With WSR-88D data, they tracked 109 cells and 26 mergers. The storms produced 39 tornadoes, with 54% occurring within 15 minutes of a cell merger. Herein, we discuss six of the mergers. We will generally use the Lee et al. designations for the cells and mergers. Tornado times, strengths, and locations are taken from *Storm Data*.

Figures 9 and 10 show supercell D12 undergoing multiple mergers. Note that ordinary cells move to the northeast, while supercells tend to move to the ENE or east. Around 2300 UTC (hereafter, all times are UTC), D10 initiates south of D12 and moves into the direct path of the supercell. D10 is quickly absorbed into D12, with little disruption to the structure of the original supercell. Coincident with the merger is the appearance of a new mesocyclone at the location where D10 is merging, with the mesocyclone associated with D12 moving to the rear of the storm and weakening (Fig. 9). During the merger process, two tornadoes are produced: One, with tornadogenesis at 2307, produces F2 damage. An F1-rated tornado begins at 2317. The D10-D12 merger resembles a Type III.

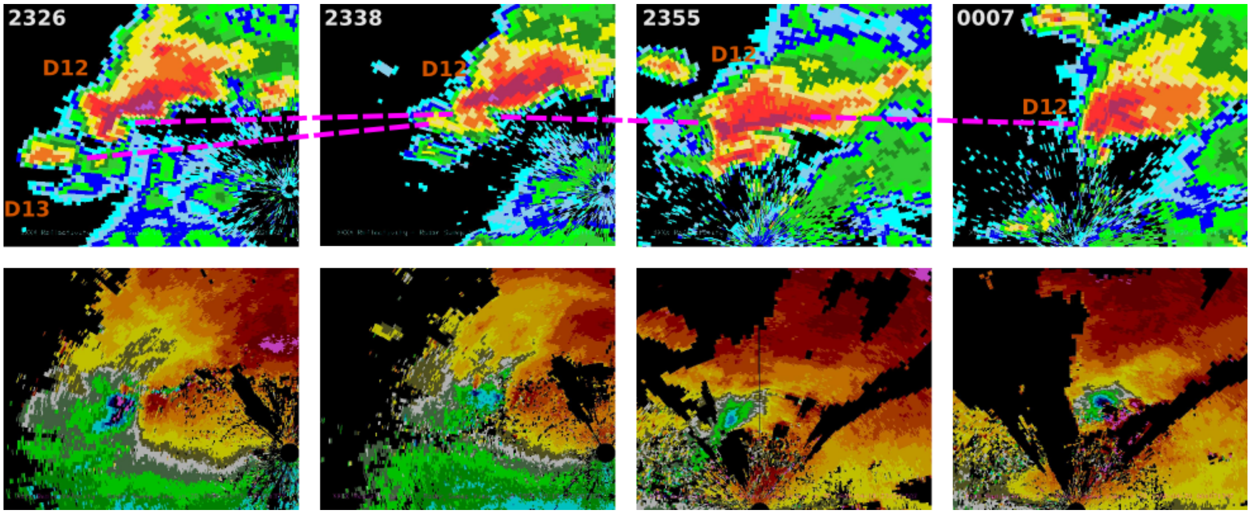

Fig. 10. As Fig. 9 for a Type IV merger. F3-rated tornado produced at 2358.

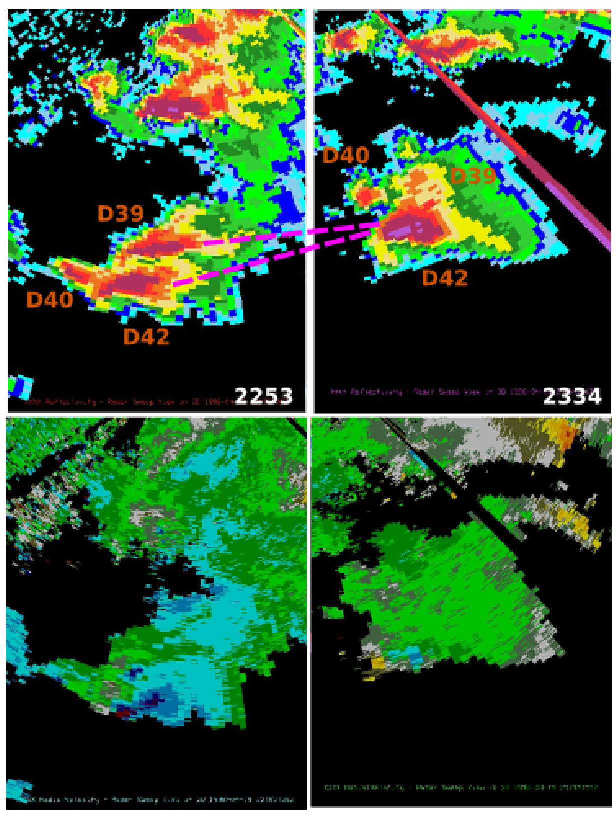

Fig. 11. As Fig. 9 from KSLX for a Type IV merger involving D42. No tornadoes are produced.

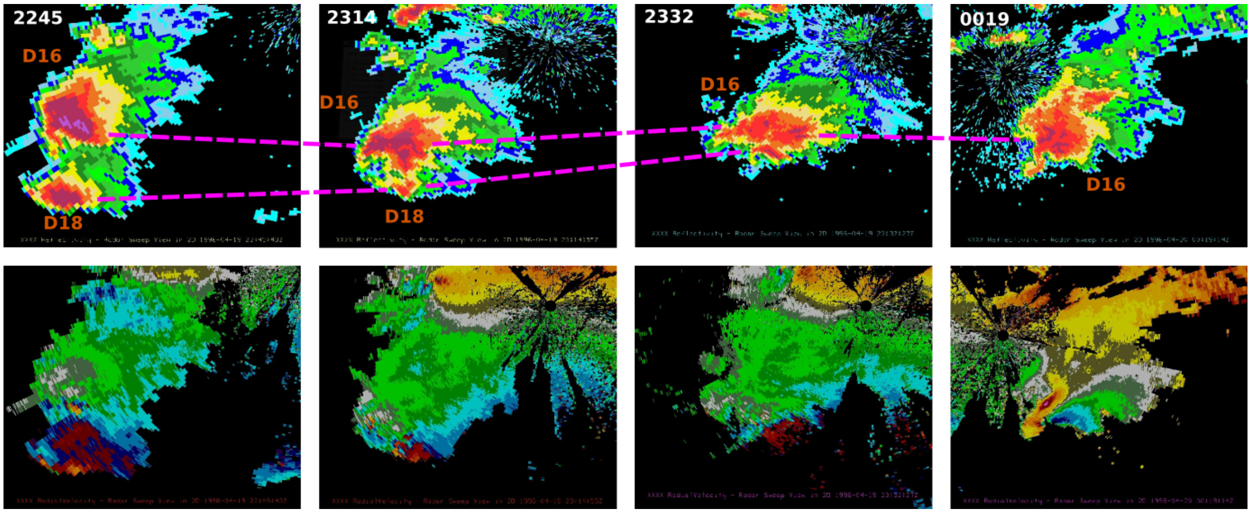

FIG. 12. As Fig. 9 from KSLX for a merger between D16 and D18. F3 tornado at 0022.

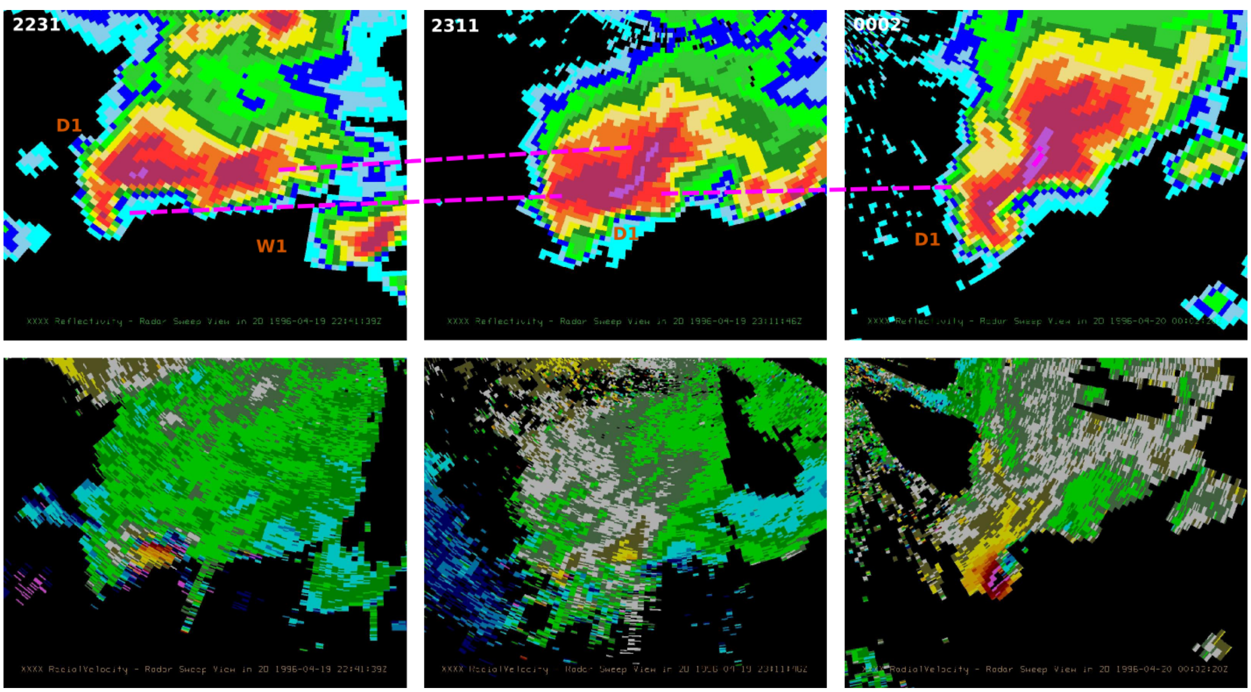

FIG. 13. As Fig. 9 from KDVN for a merger between D1 and W1. Two tornadoes are produced: F0 at 2300, F1 at 2310.

Shortly afterwards, around 2320, D13 is initiated behind D12, joining with D12 from the rear over the next fifteen minutes. The storm briefly takes on an S-shaped radar presentation around 2355, which may indicate an outflow surge triggering updraft growth. The echoes associated with the southern edge of thes tructure deepen and rejoin the main body of the supercell. Tornadogenesis occurs at 2358, associated with F3-rated damage. The storm continues as a supercell on the HP-classic area of the spectrum, with a broad hook and broad precipitation shield to its northeast, until about 0040, at which time the storm becomes disorganized. This D12-D13 merger bears a strong resemblance to the Type IV merger.

Figure 11 shows what also seems to be a Type IV merger. Unlike the D12-D13 event, this merger takes place between two supercells: D39 and D42. After 2250, the FFD of D42 rains into the BWER of D39, after which D39 dissipates and D42 continues as a supercell with a broad FFD. The post-merger mesocyclone of D42 is comparable in strength and size to the pre-merger mesocyclone, and at times stronger. No tornadoes are produced. This merger may also involve interactions with ordinary cell D40, which moves to the northeast behind D42, dissipating after 2320.

With limited observations, attempts to categorize mergers according to the schema presented herein can be problematic. Figure 12 demonstrates this. D18 initiates south of D16, and merges into its southern flank. The result is a somewhat disorganized-looking storm in which the mesocyclone associated with D18 retains its identity, replacing the one associated with D16. As the merger proceeds, D16 reflectivities decrease, as the storm becomes disorganized. This weakening of the structures orginally associated with D16, and the strengthening of D18, could result from D18 developing a cold pool as the merger occurs, which subsequently disrupts D16. Such a scenario would place this in the Type II category. The only definitive statement regarding the classification is that this merger is *not* a Type I. The post-merger storm is a supercell with tornadogenesis at 0022, resulting in F3 damage.

The final example is a FFD merger, which would fall under Type I (Fig. 13). D1 moves almost due east, when it encounters ordinary cell W1 at 2230. By 2311 the FFD has a linear reflectivity maximum, superficially resembling the morphology of Type I mergers. However, unlike the simulated cases, the system re-develops a strong mesocyclone at 0000, with little indication of bowing. Note that two brief, weak tornadoes are produced at 2300 and 2310, rated F0 and F1, respectively.

An initial evaluation of the proposed conceptual models based on comparison with these observed mergers suggest some success for types II-IV. For Type I mergers, the models do not predict the formation of a mesocyclone on the right flank.

More thorough analyses will be forthcoming in a future publication. These will include an examination of reflectivity changes at higher scan levels and comparison to those predicted by the conceptual models.

11 June 2010, Limon, CO merger during VORTEX2

On 11 June 2010, the VORTEX2 armada intercepted a supercell west of Limon, Colorado (Fig. 14). At 2336, DOW7 reported a tornado. Several teams and an independent storm spotter reported a funnel cloud at this time, with mobile mesonet Probe 7 measuring wind speeds above 30 m s^{-1} within the radar-indicated ground circulation. By 2345, DOW7 confirmed that the circulation had weakened, after which it was no longer considered tornadic. During this time, mobile mesonets indicated minimum θ_v (θ_e) perturbations of -6 K (-9 K) within the RFD as compared to values far from the storm.

After 2340, four new cells initiated to the south and southeast of the original supercell (hereafter designated “A”). Cells P and Q (Fig. 15 and Fig. 16) appeared first, and were completely absorbed by A by 0000. B and C maintained separate character in lower-level scans (0.5–2.3° in KFTG) until 0022. During this time, the echo top associated with C deepened dramatically as it merged into the rear flank of A. The depth and position of C suggest its updraft became the dominant updraft in the system. B moved into the FFD of A, and while the echo top of B did deepened as the reflectivity associated with A weakened, B seemed weaker and shallower. Note that, during the merger, neither B nor C produced low-θ_e outflow.

By 0030, the merger was complete (Fig. 17 and Fig. 18). The FFD had a distinctly linear form, with dual-Doppler observations from SR1 and SR2 suggesting an updraft along the forward-flank reflectivity gradient and a mesocyclone on the southeast flank. Surface observations from mobile mesonets and StickNets show a θ_v (θ_e) depression with a minimum of -7 K (-9 K), compared to the measurements well ahead of the storm (Fig. 17). Around 0050, DOWs and surface observations from mobile mesonets indicate a ground circulation associated with the mesocyclone, with wind speeds above 30 m s^{-1} and reports of a funnel cloud. Over the next half hour, the storm moves into an environment with unfavorable shear, and subsequently loses supercellular characteristics.

This storm undergoes multiple mergers at once, and thus cannot be classified according the scheme presented herein. However, this merger does share some features with some of the simulated mergers. The FFD interactions result in an outflow-dominated system that shares features in common with a quasi-linear convective system (i.e., is associated with a long updraft). The A-C interactions share features in common with Type III and Type IV mergers, with the updraft associated with A being replaced by that of C.

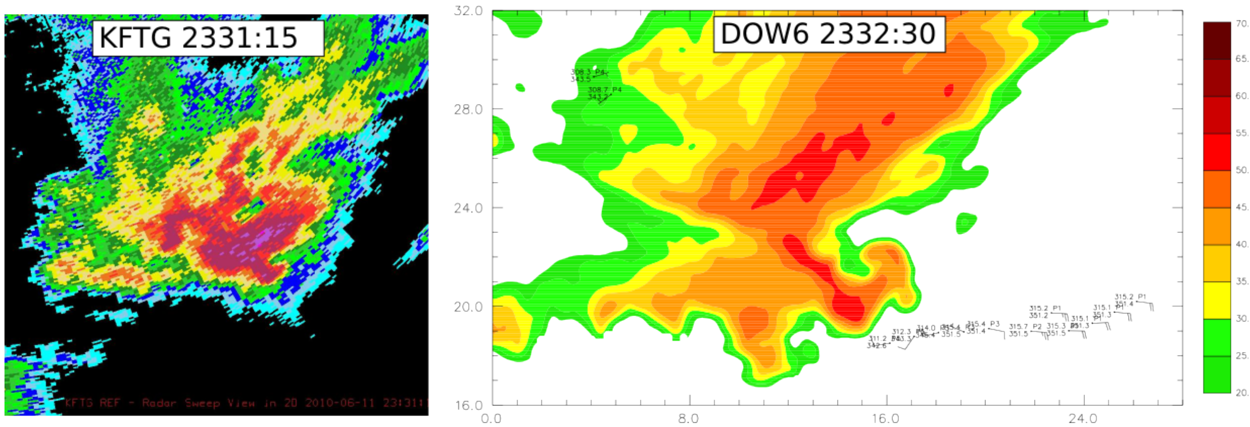

FIG. 14. KTFG (left) and DOW6 (right) reflectivity of pre-merger supercell, just before tornadic phase. Objective analysis of DOW6 used $\kappa = 0.215513$ km^2 on a grid with 100 m spacing.

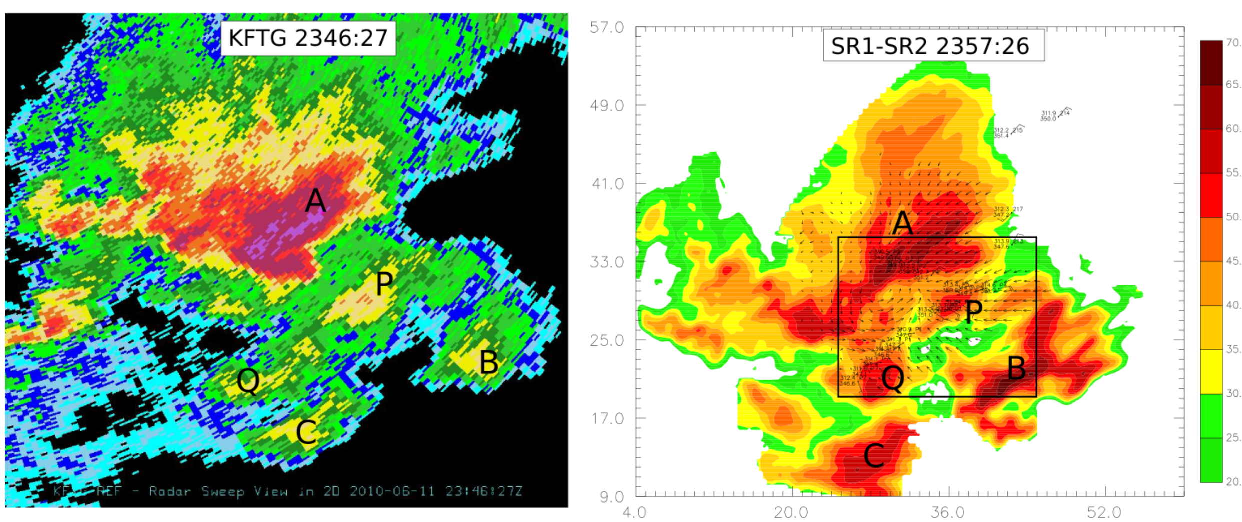

FIG. 15. KTFG (left) and dual-Doppler analysis using SR1 and SR2, with mobile mesonet station models (right). The objective analysis of SR1 and SR2 used $\kappa = 0.484905$ km^2 for a two-pass Barnes analysis on a grid with 200 m spacing. For station models, top number indicates θ_v, bottom indicates θ_e. Fig. 16 shows a close-up of the area within the black box.

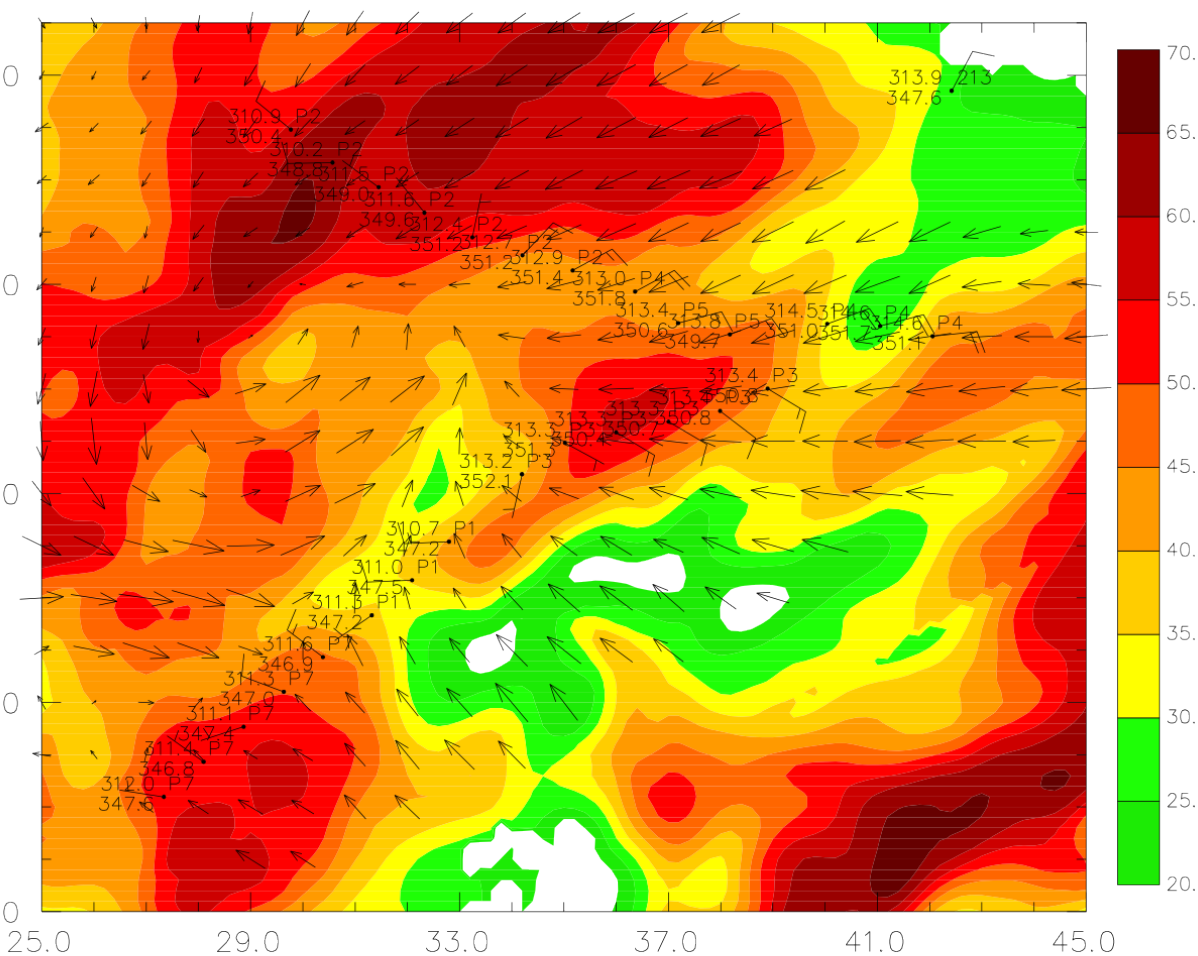

FIG. 16. Close-up of mesonet station models from Fig. 15.

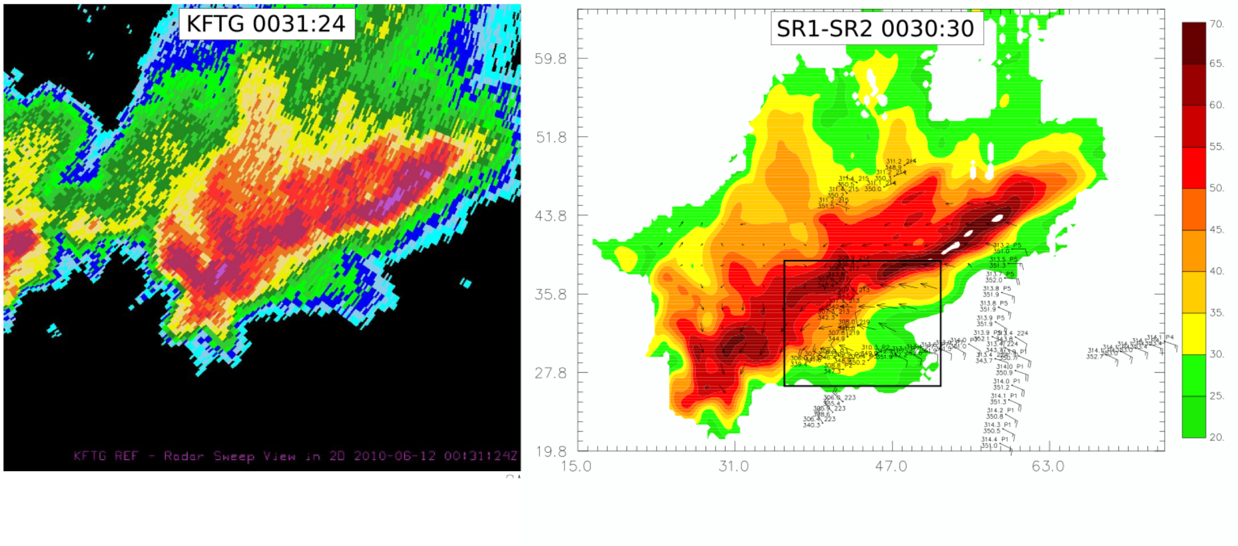

FIG. 17. Similar to Fig. 15, except station models include StickNets. Fig. 18 shows a close-up of the area within the black box.

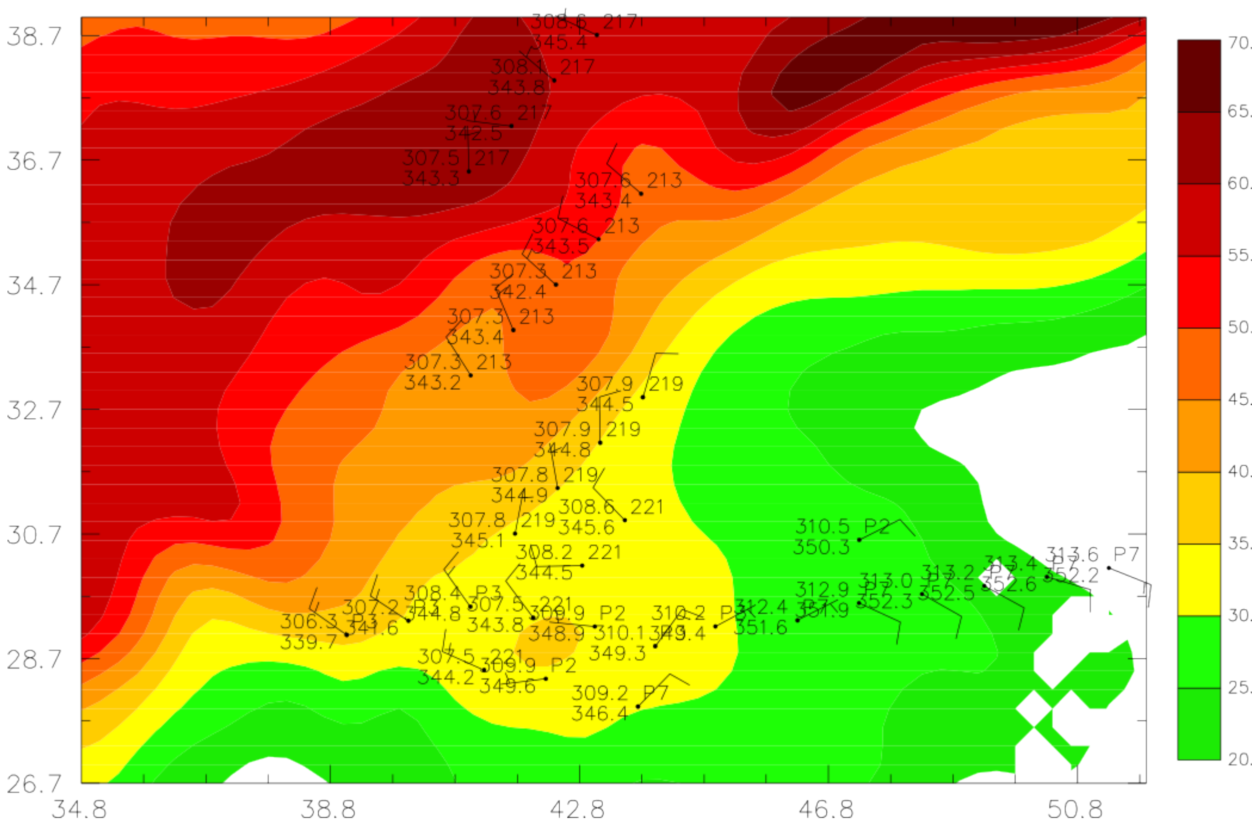

FIG. 18. Close-up of mesonet station models from Fig. 17

More thorough analyses of this case and of a merger case from 18 May 2010 (Skinner et al. 2012 and Dowell et al. 2012) will be forthcoming in a future publication.

6. Discussion

Through a suite of numerical simulations of storm mergers, varying the location and maturity of the new storm relative to the original, a general classification of merger types was identified, designated as Type I-IV. Types I and II occur when the new storm merges into the FFD of the original supercell. In Type I mergers, the system re-organizes as a bow echo. In Type II, the merger results in a classic supercell. Type III mergers occur when the updraft directly interact, resulting in the dissipation of the replacement of the original updraft and the continuation of the storm as a classic or HP supercell. Type IV mergers occur when the new cell merges into the RFD of the original, and result in HP supercells with strong mesocyclones.

These experiments were carried out in a homogenous environment with a semicircular hodograph, and thus should not be expected to exhaust all possibilities for the mode of merger. Despite this limitation, some basic dynamics that should be expected to hold across environments could be identified. Principal among these is the effect of the distribution of precipitation on the strength of the cold pool. Increasing the number concentration and overall mass of hydrometeors leads to a decrease in the buoyancy as a direct result of hydrometeor-loading and melting or evaporative cooling. In turn, this strengths the cold pool, effecting changes in the morphology of the entire system.

Initial comparisons with real-world observations provide confirmation of some aspects of the general features of the model types. Merger events that could be roughly categorized as Types II–IV resulted in supercells. The principal failure of the conceptual model is with Type I: While simulations predict a strong, cold-pool-driven bow echo, the observed reality is a linear system with a mesocyclone. This may result from a number of factors. First and foremost, the idealized nature of the model environment falls far short of the realities of heterogenous environments during tornado outbreaks. While these idealized experiments are useful for shedding light on the dynamics intrinsic to the merger process itself, mesoscale differences in actual environments are expected to have a significant impact on storm behavior (e.g., Richardson et al. 2007). Another problem is in the limitations of the model itself. Reproduction of realistic cold pools is difficult, and profoundly affected by the microphysics parameterizations used in modeling (e.g., Dawson et al. 2010). Type I storms in simulation may transition to bow echoes because the cold pools are quite simply too strong.

With this in mind, future work on the topic along both numerical and observational lines can be readily envisioned. Additional simulations in different environments (e.g., with unidirectional shear) will be helpful. A closer examination of the microphysics is also merited. For this study, we used the CM1r15 implementation of Morrison et al. (2005) microphysics, which includes a parameterization of drop break-up based on drop size of Verlinde and Cotton (1993). In the model, the maximum drop size was set to 0.9 mm, which may be too small to adequately represent deep convection.

Besides the additional simulations, comparisons to additional observations is necessary. During this process of comparison, the aspects by which the models fail to capture the realities may be identified and used to modify the models themselves. In this way, an accurate picture of the long-term effect of cell merger on storm morphology may be developed.

Acknowledgments.

We would like to thank David Dowell, Hans Verlinde, Pat Skinner, Tony Reinhart, Jim Marquis, Chris Nowotarski, Johannes Dahl, and Dan Dawson for their helpful suggestions. We would also like to thank Rachel Humphreys, Gordon Carrie, Mike Biggerstaff, Paul Robison, National Center for Atmospheric Research (NCAR), National Severe Storms Laboratory, Sherman Frederickson, Sean Waugh, George Bryan, Matt Parker, and the rest of the VORTEX2 personnel for collecting and providing data. In addition to assistance with data, George Bryan and NCAR provided the cloud model used herein. For providing code used in the radar analysis, we thank Nettie Arnott, Curtis Alexander, David Dowell and Mario Majcen. This work was supported by National Science Foundation grants NSF AGS-0801035, NSF AGS-1157646, NSF AGS-0801041, NSF AGS-0800542.

References

Biggerstaff, M., L. J. Wicker, J. Guynes, C. Ziegler, J. M. Straka, E. N. Rasmussen, A. D. Dogett IV, L. D. Carey, J. L. Schroeder and C. Weiss, 2005: The Shared Mobile Atmospheric Research and Teaching Radar: A collaboration to enhance research and teaching. *Bull. Amer. Meteor. Soc.*, **86**, 1263–1274.

Bryan, G. H., and J. M. Fritsch, 2002: A benchmark simulation for moist nonhydrostatic numerical models. *Mon. Wea. Rev.*, **130**, 2917–2928.

Dawson II, D. T., M. Xue, J. A. Milbrandt, M. K. Yau, 2010: Comparison of evaporation and cold pool development between single-moment and multimoment bulk microphysics schemes in idealized simulations of tornadic thunderstorms. *Mon. Wea. Rev.*, **138**, 1152–1171.

Dowell, D. C., C. C. Weiss, A. E. Reinhard, and P. Skinner, 2012: Baroclinicity and mesocyclogenesis in a simulation of the VORTEX2 18 May 2010 Dumas, Texas supercell. *26th Conf. on Severe Local Storms,* Nashville, TN, Amer. Meteor. Soc, 13.5.

Finley, C. A., W. R. Cotton, and R. A. Pielke, Sr., 2001: Numerical simulation of tornadogenesis in a high-precipitation supercell. Part I: Storm evolution and transition into a bow echo. *J. Atmos. Sci.*, **58**, 1597–1629.

Lee, B. D., B. F. Jewett, and R. B. Wilhelmson, 2006a: The 19 April 1996 Illinois tornado outbreak. Part I: Cell evolution and supercell isolation. *Wea. Forecasting*, **21**, 449–464.

________, 2006b: The 19 April 1996 Illinois tornado outbreak. Part II: Cell mergers and associated tornado incidence. *Wea. Forecasting*, **21**, 449–464.

Majcen, M., P. Markowski, Y. Richardson, D. Dowell and J. Wurman, 2008: Multipass objective analyses of Doppler radar data. *J. Atmos. Ocean Tech*, **25**, 1845–1858.

Morrison, H. and G. Thompson, 2009: Impact of cloud microphysics on the development of trailing stratiform precipitation in a simulated squall line: Comparison of one- and two-moment schemes. *Mon. Wea. Rev.*, **137**, 991–1007.

________, J. A. Curry, and V. I. Khvorostyanov, 2005: A new double-moment microphysics parameterization for application in cloud and climate models. Part I: Description. *J. Atmos. Sci.,* **62**, 1665–1677.

Pauley, P. M. and X. Wu, 1990: The theoretical, discrete, and actual response of the Barnes objective analysis scheme for one- and two- dimensional fields. *Mon. Wea. Rev.*, **118**, 1145–1164.

Rasmussen, E. N. and D. O. Blanchard, 1998: A baseline climatology of sounding-derived supercell and tornado forecast parameters. *Wea. Forecasting*, **13**, 1148–1164.

Richardson, Y. P., K. K. Droegemeier, and R. P. Davies-Jones, 2007: The influence of environmental variability on numerically simulated convective storms. Part I: Variations in vertical shear. *Mon. Wea. Rev.*, **135**, 3429–3455.

Rotunno, R., J. B. Klemp and M. L. Weisman, 1988: A theory for strong, long-lived squall lines. *J. Atmos. Sci.*, **45**, 463–485.

Skinner, P. S., C. C. Weiss, L. J. Wicker and C. K Potvin, 2012: VORTEX2 observations and data assimilation experiments of the 18 May 2010 Dumas, Texas supercell. *26th Conf. on Severe Local Storms*, Nashville, TN, Amer. Meteor. Soc., 13.6.

Straka, J. M., E. N. Rasmussen, and S. E. Frederickson, 1996: A mobile mesonet for finescale meteorological observations. *J. Atmos. Ocean. Tech.*, **13**, 921–936.

Verlinde, J., and W. R. Cotton, 1993: Fitting microphysical observations of nonsteady convective clouds to a numerical model: An application of the adjoint technique of data assimilation to a kinematic model. *Mon. Wea. Rev.*, **121**, 2776–2793.

Weisman, M. L. and J. B. Klemp, 1984: The structure and classification of numerically simulated convective storms in directionally varying wind shears. *Mon. Wea. Rev.*, **112**, 2479–2498.

________, J. B. Klemp, 1982: The dependence of numericall simulated convective storms on vertical wind shear and buoyancy. *Mon. Wea. Rev.*, **110**, 504–520.

Weiss, C. C., and J. L. Schroeder, 2008: Sticknet—A new, portable, rapidly-deployable, surface observing system. Preprints, *25th Int. Conf. on Interactive Information Processing Systems for Meteorology, Oceanoglaphy and Hydrology,* New Orleans, LA, Amer. Meteor. Soc., P4A.1.

Wurman, J. M., Y. P. Richardson, C. Alexander, S. Weygandt, P. F. Zhang, 2007: Dual-Doppler and single-Doppler analysis of a tornadic storm undergoing mergers and repeated tornadogenesis. *Mon. Wea. Rev.*, **135**, 736–758.

________, J. Straka, E. Rasmussen, M. Randall, and A. Zahrai, 1997: Design and deployment of a portable, pencil-beam, pulsed, 3-cm Doppler radar. *J. Atmos. Ocean. Tech.*, **14**, 1502–1512.